Biochimica et Biophysica Acta 1840 (2014) 3022–3033

Contents lists available at ScienceDirect

Biochimica et Biophysica Acta

journal homepage: www.elsevier.com/locate/bbagen

The role of frataxin in fission yeast iron metabolism: Implications for Friedreich's ataxia

Yu Wang [a], Yiwei Wang [b], S. Marcus [b], L.S. Busenlehner [a,*]

[a] Department of Chemistry, The University of Alabama, Tuscaloosa, AL 35487, USA
[b] Department of Biological Sciences, The University of Alabama, Tuscaloosa, AL 35487, USA

ARTICLE INFO

Article history:
Received 25 February 2014
Received in revised form 25 June 2014
Accepted 26 June 2014
Available online 3 July 2014

Keywords:
Friedreich's ataxia
Frataxin
Iron–sulfur cluster
Iron homeostasis

ABSTRACT

Background: The neurodegenerative disease Friedreich's ataxia is the result of frataxin deficiency. Frataxin is a mitochondrial protein involved in iron–sulfur cluster (Fe–S) cofactor biogenesis, but its functional role in this pathway is debated. This is due to the interconnectivity of iron metabolic and oxidative stress response pathways that make distinguishing primary effects of frataxin deficiency challenging. Since Fe–S cluster assembly is conserved, frataxin overexpression phenotypes in a simple eukaryotic organism will provide additional insight into frataxin function.

Methods: The *Schizosaccharomyces pombe* frataxin homologue (*fxn1*) was overexpressed from a plasmid under a thiamine repressible promoter. The *S. pombe* transformants were characterized at several expression strengths for cellular growth, mitochondrial organization, iron levels, oxidative stress, and activities of Fe–S cluster containing enzymes.

Results: Observed phenotypes were dependent on the amount of Fxn1 overexpression. High Fxn1 overexpression severely inhibited *S. pombe* growth, impaired mitochondrial membrane integrity and cellular respiration, and led to Fxn1 aggregation. Cellular iron accumulation was observed at moderate Fxn1 overexpression but was most pronounced at high levels of Fxn1. All levels of Fxn1 overexpression up-regulated oxidative stress defense and mitochondrial Fe–S cluster containing enzyme activities.

Conclusions: Despite the presence of oxidative stress and accumulated iron, activation of Fe–S cluster enzymes was common to all levels of Fxn1 overexpression; therefore, Fxn1 may regulate the efficiency of Fe–S cluster biogenesis in *S. pombe*.

General Significance: We provide evidence that suggests that dysregulated Fe–S cluster biogenesis is a primary effect of both frataxin overexpression and deficiency as in Friedreich's ataxia.

1. Introduction

Friedreich's Ataxia (FA) is one of the most common autosomal recessive ataxias in Caucasians, with a prevalence of 2–4 patients per 100,000 individuals [1]. The major clinical features of FA include progressive ataxia, cardiomyopathy, atrophy of the spinal cord and diabetes [2]. The hallmarks of FA development include increased mitochondrial iron content, oxidative stress, and deficient activities of iron–sulfur (Fe–S) cluster enzymes in mitochondria of affected tissues [3]. FA is most commonly caused by an expanded GAA repeat in the first intron of the *fxn* gene that encodes the mitochondrial protein frataxin [4]. This genomic change is responsible for reduced *fxn* mRNA levels and decreased expression of functional frataxin protein [5]. Currently, there is no cure for FA. Gene therapy and other treatments have shown promising results, but more knowledge of frataxin functional pathways is required [6].

Frataxin is highly conserved with homologues in all eukaryotes and many prokaryotes [2]. Three-dimensional structures of human frataxin (hFxn) and both *S. cerevisiae* (Yfh1) and *E. coli* (CyaY) frataxin homologues revealed a unique structural fold, suggesting that frataxin function(s) might be evolutionarily conserved [7–9]. Early pathophysiological studies and phylogenetic studies of FA patients and tissues demonstrated that frataxin has a critical role in Fe–S cluster biogenesis, but the exact role remains elusive [10,11]. One hypothesis is that

Abbreviations: FA, Friedreich's ataxia; Fe–S, iron–sulfur; hFxn, human frataxin; Yfh1, *S. cerevisiae* frataxin homologue; CyaY, *E. coli* frataxin homologue; Nfs1, cysteine desulfurase; Isu1, iron sulfur scaffold protein; Isd11, Fe–S accessory protein; *nmt1*, no message in thiamine promoter; EMM, Edinburgh minimal media; SDH2, succinate dehydrogenase; *sdh2-GFP*, green fluorescent protein fused-SDH2; qRT-PCR, quantitative real-time PCR; BCA, bicinchoninic acid; BPS, bathophenanthrolinedisulfonic acid; $NADP^+$/NADPH, nicotinamide adenine dinucleotide phosphate; PMS, phenazine methosulfate; DCIP, 2,6-dichlorophenolindophenol; SOD, *S. pombe* superoxide dismutase; Fxn1Δ2–11, *S. pombe* Fxn1 with deletion of residues 2–11; MALDI-TOF, matrix assisted laser desorption ionization time of flight; Frp1, *S. pombe* ferric reductase; DTPA, diethylene triamine pentaacetic acid; DFO, deferoxamine; TCA, citric acid cycle; ROS, reactive oxygen species

* Corresponding author at: Department of Chemistry, The University of Alabama, Box 870336, Tuscaloosa, AL 35487, USA. Tel.: +1 205 348 0269; fax: +1 205 348 9104.
E-mail addresses: smarcus@ua.edu (S. Marcus), LSBusenlehner@ua.edu (L.S. Busenlehner).

http://dx.doi.org/10.1016/j.bbagen.2014.06.017
0304-4165/

frataxin is the iron chaperone for Fe–S cluster biogenesis by the ternary biosynthetic complex composed of the cysteine desulfurase Nfs1, the Fe–S cluster scaffold protein Isu1, and the accessory protein Isd11. Frataxin interacts with both Nfs1 and Isu1 in humans and *S. cerevisiae* [12,13] and can transfer iron to Isu1 *in vitro* [13,14]. Another hypothesis is that frataxin allosterically regulates Fe–S cluster biosynthesis via Nfs1; however, a full understanding of how frataxin modulates Nfs1 activity is lacking [15,16]. It is also possible that frataxin could have other functions, such as maturation of cellular Fe–S proteins [11,17,18], repair of Fe–S cluster containing proteins [19], iron storage [20], and iron donation to the heme biosynthesis enzyme ferrochelatase [21].

Most *in vivo* studies of frataxin and its homologues mimic FA through reduced levels of frataxin expression in target cells or organisms [10,20,22–24]. These experiments have provided great insight into the possible functions of frataxin in mitochondrial iron metabolism, but the phenotypes are complex. Because iron metabolism is a delicately controlled system, distinguishing which observed effects are directly related to frataxin depletion and not indirect effects of imbalanced iron metabolism has been challenging [25]. However, characterizing the phenotypes of frataxin overexpression in a simple and well-studied organism provides complementary knowledge to frataxin function. Although frataxin overexpression studies do not correspond to a model for FA, these studies help decipher its role in iron metabolic pathways and may also provide expression-level information important to potential gene therapy applications. Frataxin overexpression studies have been performed with *S. cerevisiae*, *D. melanogaster*, *M. musculus*, and human cell lines (Table 1); however, the human cells and mouse models have given contradictory results compared to those of fly and yeast in terms of Fe–S cluster enzyme activities, oxidative stress, and cell viability [10,26–29]. Due to the possible differences in iron homeostasis between higher eukaryotes and budding yeast, the fission yeast *Schizosaccharomyces pombe* was chosen as a model system to study the *in vivo* impacts of frataxin overexpression since it is thought to be evolutionarily more similar to mammalian cells than *S. cerevisiae* [30,31]. Since frataxin overexpression levels were not determined or varied between model organisms [10,26–29], phenotypic characterization from several overexpression levels is required to properly interpret the role of frataxin in iron metabolism.

S. pombe has the smallest number of protein coding genes yet reported for a sequenced eukaryotic genome [32]. Genetic manipulation is straightforward and well described. For the present study, a *S. pombe* strain was created in which the *S. pombe* frataxin homologue Fxn1 (also named Pfh1 [33]) was overexpressed from a plasmid under the control of the thiamine repressible *nmt1* promoter [34,35]. Surprisingly, high overexpression of Fxn1 inhibits cell growth and perturbs mitochondrial function in *S. pombe*. Despite iron accumulation and possible oxidative stress, activities of Fe-S enzymes aconitase and succinate dehydrogenase were significantly increased. The results of this study support the hypothesis that *S. pombe* Fxn1 enhances Fe–S cluster biogenesis or maturation of Fe–S cluster proteins. This further suggests that frataxin deficiency would primarily lead to decreased production of Fe–S clusters and Fe–S containing proteins that are essential for cell viability and function [36].

2. Materials and methods

2.1. Yeast strains, plasmid construction, and growth media

2.1.1. Yeast strains

Schizosaccharomyces pombe strains used in this study were SP870 (*h*^{90} *ade6-210 leu1-32 ura4-D18*) (from D. Beach) and sdh2-GFP (*h*^{90} *ade6-M210/216** *ura4-D18 leu1-32 sdh2::GFP::KanMX6*) (this study). *S. pombe* transformants were grown in Edinburgh minimal medium (EMM) with 250 mg/l adenine and uracil (EMM + AU). *S. pombe* cells were transformed with indicated plasmids using the standard lithium acetate procedure [37].

2.1.2. Plasmid construction

Plasmids used in this study were pREP3X [34], pREP3X/Fxn1, pREP3X/Fxn1Δ2–11, and pREP3X/Fxn1-6His, pREP4X, and pREP4X/Isu1. The coding sequence of *fxn1* from *S. pombe* genomic DNA was amplified by PCR and ligated into pREP3X between the *Bam*HI and *Xho*I sites to produce pREP3X/Fxn1. Plasmids pREP3X/Fxn1Δ2–11 and pREP3X/Fxn1-6His were constructed in pREP3X/Fxn1 by deleting the base pairs encoding amino acid residues 2–11 in the *fxn1* sequence or by inserting the 6His coding sequence (5′-CATCATCATCATCATCAT-3′) at the 3′-end of *fxn1* using QuikChange Lighting site-directed mutagenesis (Agilent Technologies). The coding sequence of *isu1* was amplified from *S. pombe* genomic DNA by standard PCR and ligated into pREP4X between the *Bam*HI and *Xho*I sites, to produce the pREP4X/Isu1 plasmid.

2.1.3. Cell cultures

S. pombe cells transformed with plasmids pREP3X, pREP3X/Fxn1, pREP3X/Fxn1Δ2–11, or pREP3X/Fxn1-6His were maintained on EMM + AU agar with 50 μM thiamine. Each transformant was grown overnight in EMM + AU with 50 μM thiamine at 30 °C with shaking to mid-log phase. Cells were harvested by centrifugation and the cell pellets were washed twice with EMM + AU before inoculation into fresh EMM + AU medium containing 50 μM, 50 nM or 10 nM thiamine [38]. All cultures were grown at 30 °C for 72 h and cells were sub-cultured into fresh medium when necessary to maintain a cell density of $\leq 1 \times 10^7$ cells/ml, which is mid-logarithmic for *S. pombe* growth. Samples for all assays are prepared from the final cultures unless specifically indicated.

Table 1
The major observations of frataxin overexpression in different organisms.

Frataxin	Organism/cell lines	Amount of overexpression	Major observations	Reference
Human FXN1	Human preadipocytes	2–8-fold	Increased cellular respiration; increased oxidative phosphorylation	Ristow et al. [68]
Human FXN1	Human colon carcinoma	N.D.[a]	Decreased cellular growth rate; increased cellular respiration; increased aconitase activity	Schulz et al. [70]
Human FXN1	Transgenic mouse	N.D.	Increased aconitase activity; up-regulated TCA cycle	Pook et al. [72]
Human FXN1	Transgenic mouse	4–10-fold	No change in systemic iron metabolism; (no measurement of aconitase or respiration)	Miranda et al. [26]
Human FXN1	Transgenic *Drosophila* model	9 fold	Reduced viability; increased sensitivity to oxidative stress; decreased aconitase activity; increased oxidative stress	Navarro et al. [29]
Drosophila Dfh1	Transgenic *Drosophila* model	9 fold	Developmental defects; no change in aconitase activity	Llorens et al. [71]
Drosophila Dfh1	Transgenic *Drosophila* model	3–5-fold	Increased total antioxidant activity; resistance to oxidative stress	Runko et al. [27]
Yeast Yfh1	*S. cerevisiae*	2–18-fold	Iron accumulation; decreased SDH and aconitase activities; impaired respiration; increased resistance to oxidative stress	Seguin et al. [28]

[a] Not determined.

2.2. Growth assays

Growth of pREP3X, pREP3X/Fxn1, pREP4X, and pREP4X/Isu1 transformants was analyzed with serial dilution spotting assays. An overnight culture for each transformant was grown to mid-log phase in EMM + AU (pREP3X transformants) or EMM + AL (pREP4X transformants) with 50 μM thiamine at 30 °C, then cells were washed twice with EMM + AU/AL and grown in fresh EMM + AU/AL for 24 h at 30 °C with shaking. The cells were washed and serially diluted to 1×10^7, 2×10^6, 4×10^5, 8×10^4, and 1.6×10^4 cells/ml. Three microliters of the dilutions were spotted on EMM + AU/AL agar plates with thiamine and/or additional supplements, as indicated, and grown at 30 °C in either aerobic or anaerobic conditions (i.e., an O_2-deficient chamber). Photographs were taken after 3 and 5 days, which were optimal for *S. pombe* growth on minimal media [35].

2.3. Respiration rate assays

The respiration rates of the pREP3X and pREP3X/Fxn1 transformants with 50 μM, 50 nM or 10 nM thiamine were measured with Strathkelvin Model 782 dissolved oxygen measuring system coupled with Clark-type microcathode oxygen electrode [39]. The instrument was calibrated before use. One milliliter (1×10^7 cells/ml) of each final culture was added to the cuvette and the oxygen concentration was recorded once the reading was stable and repeated after 5 min. The oxygen consumption rate was calculated as ng/(ml·min) per 10^6 cells.

2.4. Analysis of mitochondrial organization

Mitochondrial organization was visualized by fluorescence microscopy using an *sdh2-GFP* strain in which the protein coding sequence of the mitochondrial-localized succinate dehydrogenase-2 gene (*sdh2*) is fused at its 3′ end to the coding sequence for green fluorescent protein (GFP) [40]. *Sdh2-GFP* cells transformed with pREP3X/Fxn1 or pREP3X were cultured under the same conditions as SP870 transformants. Fluorescence microscopy of *sdh2-GFP* transformants was carried out using a Nikon 90i automated epifluorescence microscope system equipped with a 60× Plan Fluor objective lens and operated using Nikon NIS-Elements software. Images of fluorescent cells were captured using a Photometrics CoolSNAP HQ2 monochrome CCD camera. Raw images were level-adjusted using Adobe PhotoShop CS5.

2.5. mRNA isolation, cDNA synthesis, and quantitative real-time PCR (qRT-PCR)

Three transformants of pREP3X and pREP3X/Fxn1 were each cultured in EMM + AU with 50 μM, 50 nM or 10 nM thiamine for 72 h at 30 °C. For the 3 biological replicates, total RNA was extracted using the Ambion RiboPure Yeast kit. The RNA concentration and purity were determined using an Agilent 8453 UV-visible spectrometer ($A_{260}/A_{280} \geq 2.1$, $A_{260}/A_{230} \geq 1.5$). The integrity of total RNA was verified by a 1.5% TAE-agarose gel. The synthesis of cDNA from 1 μg extracted total RNA was performed using the Quanta qScript kit.

Quantitative RT-PCR was performed using Quanta PerfeCta SYBR Green Supermix in a Bio-Rad MyiQ real-time PCR detection system. Three technical replicates were performed for each biological replicate. The primers for assayed genes are listed in Table S1 in the Supplementary data. The cycling conditions were 95 °C for 3 min, followed by 40 cycles of 95 °C (10 s) and then 58 °C (30 s). A melt curve analysis was performed to ensure that a single PCR product was amplified and detected. Three technical replicates were performed for each sample. The relative expression levels were calculated using the actin *act1* housekeeping gene as the reference [24] according to Eqs. (1) and (2) where C_T is the threshold cycle for target amplification [41].

$$-\Delta\Delta C_T = \left[C_{T(\text{gene})} - C_{T(\text{actin})}\right]_{(\text{pREP3x/Fxn1})} - \left[C_{T(\text{gene})} - C_{T(\text{actin})}\right]_{(\text{pREP3X})} \quad (1)$$

$$\text{Relative mRNA expression} = 2^{-\Delta\Delta C_T} \quad (2)$$

2.6. Cellular fractionation

2.6.1. Whole cell lysate preparation

Mid-log phase cultures of pREP3X or pREP3X/Fxn1 transformants were harvested by centrifugation at 3000 ×*g* for 5 min at 4 °C, then the cell pellets were resuspended with Chelex-treated phosphate buffered saline (pH 7.4) with 1 mM phenylmethanesulfonyl fluoride and 1 mM benzamidine to a final density of 2×10^9 cells/ml. Cells were vigorously vortexed with acid-washed glass beads at 4 °C. The total protein concentrations of the cell lysates were determined by the Thermo Pierce bicinchoninic acid (BCA) assay.

2.6.2. Isolation of mitochondria

Mitochondria were purified from pREP3X or pREP3X/Fxn1 transformants grown in 50 μM, 50 nM, or 10 nM thiamine for 72 h according to Chiron *et al.* with minor changes [42]. Purified mitochondria were resuspended in 10 mM imidazole (pH 6.4) with 0.6 M sorbitol. Total protein concentration of the cell homogenate, the homogenate post-mitochondrial separation, and the isolated mitochondria were determined by the BCA assay.

2.7. Immunodetection of Fxn1-6His

Ten micrograms of isolated mitochondrial protein in 0.5% Tween-20 and 10% glycerol was separated on a 15% SDS-PAGE gel. Protein was transferred to a nitrocellulose membrane and blocked with 5% BSA. Fxn1-6His was detected with mouse monoclonal His-tag primary antibody (Abgent) and goat anti-mouse IgG/alkaline phosphatase conjugate secondary antibody (Southern Biotech) using nitroblue tetrazolium/5-bromo-4-chloro-3′-indolyl phosphate (NBT/BCIP) staining. Analysis of Fxn1-6His expression levels and distribution was performed using the UVP MultiDoc-It imaging system and ImageJ software (NIH). Images were level-adjusted using Adobe Illustrator CS3.

2.8. Iron content

Total iron content of cell lysate and isolated mitochondria of pREP3X and pREP3X/Fxn1 *S. pombe* cells cultured in EMM + AU (740 nM iron) with no additional iron added was determined with bathophenanthrolinedisulfonic acid (BPS) [43]. Cells (10 ml of cells from a 1×10^7 cells/ml culture) from transformants grown in 50 μM, 50 nM or 10 nM thiamine were lysed and the final volume was adjusted to 200 μl. One hundred microliters of each sample was acidified with 60 μl of concentrated HCl and heated at 100 °C for 15 min. For mitochondrial iron, 0.5 mg of isolated mitochondria was disrupted with 0.5% Triton X-100 in Chelex-treated water up to 100 μl and incubated on ice for 5 min. Samples were acidified with 60 μl concentrated HCl and heated at 100 °C for 15 min. For both lysate and mitochondrial extracts, precipitate was removed by centrifugation at 14,000 rpm for 5 min. Then, 100 μl of supernatant was added to 650 μl of 0.5 M Tris–HCl (pH 8.5), 100 μl of fresh 5% ascorbate, and 200 μl of 0.1% BPS. The sample was incubated for 1 h at 23 °C and the total iron concentration was determined by the absorbance at 535 nm using an Agilent 8453 UV-visible spectrophotometer. A standard calibration curve of iron (4.5–107.4 μM) was prepared from serial dilutions using a calibrated iron solution (Perkin Elmer).

2.9. Enzyme activity assays

Enzyme activities are reported as the change in the concentration of product formed per unit of time per amount of total mitochondrial protein. While standard practice, normalization of enzyme activity to total mitochondrial protein does not reflect possible changes in protein levels as a result of Fxn1 overexpression.

2.9.1. Aconitase activity assay

Twenty-five micrograms of isolated mitochondria was resuspended with 100 μl of buffer (50 mM Tris–HCl, 0.5 mM $MnCl_2$, 30 mM sodium citrate, 0.5% Triton X-100, pH 7.4) at 4 °C, essentially as described by Pierik et al. [44]. Fifty microliters (12.5 μg) was added to 50 μl of 50 mM Tris–HCl, 0.5 mM $MnCl_2$, 1 mM sodium citrate, and 1 mM L-cysteine at pH 7.4 and loaded to Greiner 96-well plate. The reaction was initiated with 100 μl of 5 mg/ml $NADP^+$ with 8 units/ml isocitrate dehydrogenase. The formation of NADPH was followed at 340 nm for 30 min at 37 °C using a BioTek Synergy 2 Multi Detection microplate reader. The extinction coefficient for NADPH is $\Delta\varepsilon_{340} = 0.06622\ \mu M^{-1}\ cm^{-1}$. The relative aconitase activity was normalized to the amount of total protein in the reaction.

2.9.2. Succinate dehydrogenase activity assay

Fifty micrograms of isolated mitochondria was diluted to 1 ml with cold buffer (50 mM Tris–HCl pH 7.4, 10 μg/ml antimycin A, 1 mM $CaCl_2$, 1 mM KCN, 8 mg/ml sodium succinate) and incubated for 5 min, as described by Ackrell *et al.* [45]. The solution was heated to 37 °C in a quartz cuvette. The SDH reaction was initiated with 100 μl of 0.33% phenazine methosulfate (PMS) and 10 μl of 1% 2,6-dichlorophenolindophenol (DCIP) at 37 °C. Absorbance at 600 nm was monitored with a Cary 100 UV-visible spectrophotometer for 15 min. The decrease in absorbance at 600 nm was related to the reduction of DCIP where $\Delta\varepsilon_{600\ nm} = 0.021\ \mu M^{-1}\ cm^{-1}$. The relative SDH activity was normalized to the amount of total protein in the reaction. For this assay of SDH activity, antimycin A and potassium cyanide were added to block the normal path of electrons through the respiratory chain; therefore, the intrinsic activity of SDH is measured, which is not a reflection of total respiratory function [46]. This activity is instead related to the Fe–S cluster content [47].

2.9.3. Superoxide dismutase activity assay

Total superoxide dismutase (SOD) activity was determined with the colorimetric Sigma SOD activity assay kit according to product instructions. Each reaction contained ~5 μg of total protein from lysate of each transformant grown under the various thiamine conditions. The substrate was WST-1 (2-(4-iodophenyl)-3-(4-nitrophenyl)-5-(2,4-disulfophenyl)-2H-tetrazolium, which forms a colored formazan dye ($\lambda_{max} = 450$ nm) upon reduction by the superoxide anion. The SOD activity was quantified by measuring the decrease in the color development at 450 nm for 30 min using Greiner Bio one 96-well plates and a BioTek microplate reader. The SOD activity was normalized to the amount of total protein in the reaction.

2.9.4. Catalase activity assay

The total catalase activity was determined with the Cayman Chemical catalase assay kit, using Greiner Bio one 96-well plates and a BioTek microplate reader. Samples contained ~2 μg of total protein from cell lysate. The formation of formaldehyde was followed at 540 nm. One unit of catalase activity equals the production of 1 nmol/ml formaldehyde per min, and results are normalized to the amount of total protein.

2.10. Statistical analysis

Results are presented as means ± S.E.M. (standard error of the means), as indicated. The Student's *t*-test was used for comparison between the pREP3X control and pREP3X/Fxn1 overexpression groups and between thiamine levels in an experiment using KaleidaGraph (Synergy Software). The level of significance was set at $p \leq 0.05$ (*) and $p \leq 0.01$ (**).

3. Results

3.1. S. pombe growth effects from Fxn1 overexpression

To examine the overall cellular effects of Fxn1 overexpression in *S. pombe*, the aerobic growth of transformants with pREP3X or pREP3X/Fxn1 was analyzed with spotting assays on minimal media agar containing varying amounts of thiamine. The expression of Fxn1 from the pREP3X/Fxn1 plasmid is under the control of the thiamine repressible *nmt1* promoter, which is maximally repressed at thiamine concentrations greater than 0.5 μM and maximally de-repressed in the absence of thiamine [34,35]. Marked growth inhibition of *S. pombe* cells is correlated to the level of Fxn1 overexpression, with the greatest inhibition observed when pREP3X/Fxn1 is fully de-repressed in the absence of thiamine (Fig. 1A). Interestingly, growth of transformants overexpressing truncated Fxn1 with a disrupted mitochondrial localization sequence (Fxn1Δ2–11) is similar to pREP3X at all concentrations of thiamine (Fig. 1A). These observations demonstrate that the growth inhibition resulting from Fxn1 overexpression is related to mitochondrial levels or improper processing of Fxn1. The Fe–S cluster scaffold protein Isu1, which interacts directly with frataxin [48], was also overexpressed to determine if the Fxn1 growth inhibition is a general feature of mitochondrial protein overexpression in *S. pombe*. Slight decrease in cell viability is observed at the highest Isu1 concentrations without thiamine (Fig. 1B).

3.2. Mitochondrial integrity and cellular respiration of cells overexpressing Fxn1

To determine whether Fxn1 overexpression affects cell morphology or mitochondrial organization, pREP3X/Fxn1 and pREP3X were transformed into an *S. pombe* strain, *sdh2-GFP*, in which the gene encoding mitochondrial-localized succinate dehydrogenase (*sdh2*) is fused at its 3′-end to the protein coding sequence for green fluorescent protein (GFP). At the moderate levels of Fxn1 overexpression (50 nM thiamine) some cells have a bottle-shape appearance, which becomes more pronounced at 10 nM thiamine (Fig. 1C). Similar to mitochondria in mammalian cells [49,50], mitochondria in interphase *S. pombe* cells are organized into tubular networks that typically span the length of the cell [42,51]. As shown in Fig. 1D, pREP3X transformed *sdh2-GFP* cells exhibit predominantly normal tubular mitochondrial organization in each thiamine concentration, as did pREP3X/Fxn1 transformed cells cultured in 50 μM thiamine. At moderate Fxn1 overexpression levels, 33% of cells contain normal tubular mitochondria, which decreases to less than 10% at high Fxn1 expression (Fig. 1E) [23,52]. Anaerobic Fxn1 overexpression in 50 and 10 nM thiamine slightly increased cell viability (Fig. 1A), consistent with mitochondrial dysfunction. Further, cells cultured in 10 nM thiamine have an 80% reduction in the rate of cellular respiration, but respiration rates are reproducibly increased in cells overexpressing lower levels of Fxn1 (Fig. 1F). Thus, Fxn1 overexpression in *S. pombe* disrupts mitochondrial integrity and function when in vast excess. To determine the relative levels of oxidative stress, control and Fxn1 overexpression cells in the absence of thiamine were treated with the intracellular superoxide indicator dihydroethidium [53]. Bright fluorescence staining upon oxidation to oxyethidium is observed for cells expressing high levels of Fxn1 compared to control cells, suggestive of oxidative stress at high levels of Fxn1 (Supplementary Fig. S1).

3.3. Fxn1 overexpression levels

The relative amount of *fxn1* transcript expressed from both the *fxn1* chromosomal locus and pREP3X/Fxn1 as a function of thiamine

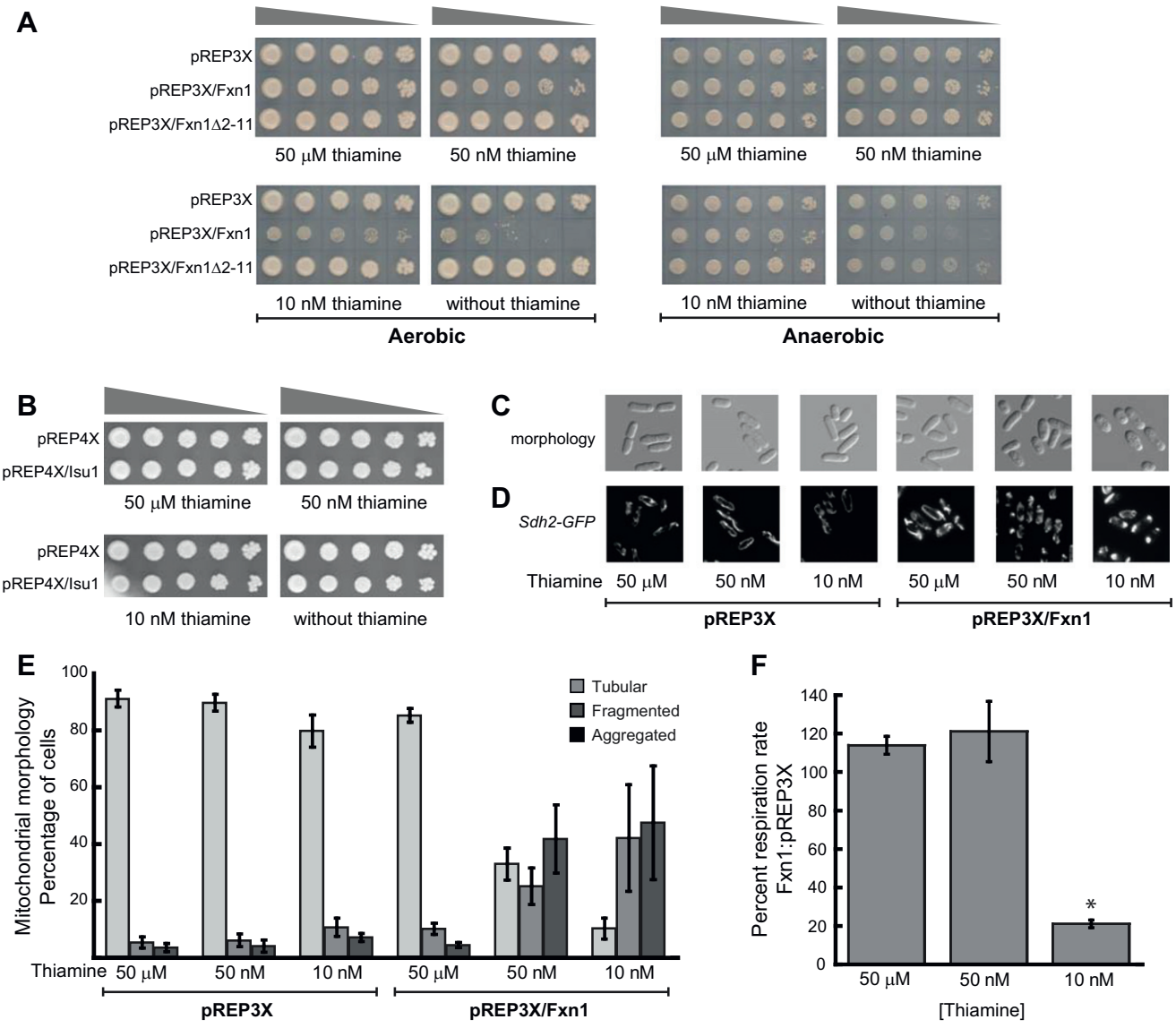

Fig. 1. *S. pombe* Fxn1 overexpression is inhibitory to cell growth and mitochondrial function. (A) *S. pombe* wild-type cells with pREP3X, pREP3X/Fxn1 or pREP3X/Fxn1Δ2–11 were grown to mid-log phase in EMM + AU without thiamine then resuspended to 1×10^7cells/ml. Cells were serially diluted (1:5) and 3 μl was spotted on EMM + AU with 0 nM, 10 nM, 50 nM and 50 μM thiamine, as indicated. Plates were incubated at 30 °C for 5 days aerobically (left) or in an anaerobic chamber (right). (B) *S. pombe* wild-type cells with pREP4X and pREP4X/Isu1 were grown to mid-log phase in EMM + AL without thiamine then resuspended to 1×10^7cells/ml. Cells were serially diluted (1:5) and 3 μl was spotted on EMM + AL with 0 nM, 10 nM, 50 nM and 50 μM thiamine, as indicated. Plates were incubated aerobically at 30 °C for 5 days. (C) Wild-type cells transformed with pREP3X/Fxn1 or pREP3X were cultured to mid-log phase and the cell morphology of representative samples was visualized by microscopy. (D) *S. pombe sdh2-GFP* cells transformed with pREP3X/Fxn1 or pREP3X were cultured under the same conditions as in (A) and were visualized for mitochondrial integrity by epifluorescence microscopy. (E) The mitochondrial membrane integrity appearance was quantified as normal, fragmented, or aggregated. Supplementary Table S2 has further sub-classifications of mitochondrial appearance. (F) Respiration rates of 1×10^7 cells/ml of wild-type pREP3X or pREP3X/Fxn1 cells in 10 nM, 50 nM and 50 μM thiamine, as indicated. The oxygen consumption rate was calculated as ng/(ml·min) per 10^6 cells (Supplementary Table S3). The data are normalized to the pREP3X transformant controls ($^*p < 0.05$; error bars shown as mean ± S.E.M., $n \geq 4$).

concentration was measured with quantitative real-time PCR (qRT-PCR) (Fig. 2A). The *nmt1* promoter is leaky [34], so *fxn1* mRNA levels are ~14-fold higher than pREP3X control transformants at 50 μM thiamine. As the thiamine concentration decreases, the *fxn1* transcript levels increase to 42- and 386-fold in 50 and 10 nM thiamine, respectively.

Mitochondria from pREP3X/Fxn1-6His transformants were isolated from cells cultured in the various thiamine concentrations. Western immunoblots of isolated mitochondria detected a ~14 kDa Fxn1-6His protein at all thiamine concentrations (Fig. 2B). As the thiamine concentration is lowered, expression of the ~14 kDa Fxn1 protein increases and at 10 nM thiamine, a ~19 kDa protein is also observed. The ~14 kDa protein was purified and MALDI-TOF mass spectrometry indicated a monoisotopic mass of 14,669 Da, which corresponds to Fxn1 residues 38–158 with the C-terminal His-tag (Supplementary Fig. S2). Thus, the first 37 amino acid residues are removed during maturation, and the high overexpression of Fxn1 leads to incomplete processing to the "mature" form. Native acrylamide gel electrophoresis shows a new diffuse band with slower electrophoretic mobility than the 14 kDa Fxn1 monomer at 10 nM thiamine, but the monomeric form is predominant (Supplementary Fig. S3). No evidence of post-translational modifications for either the 14 or 19 kDa proteins is observed (Supplementary

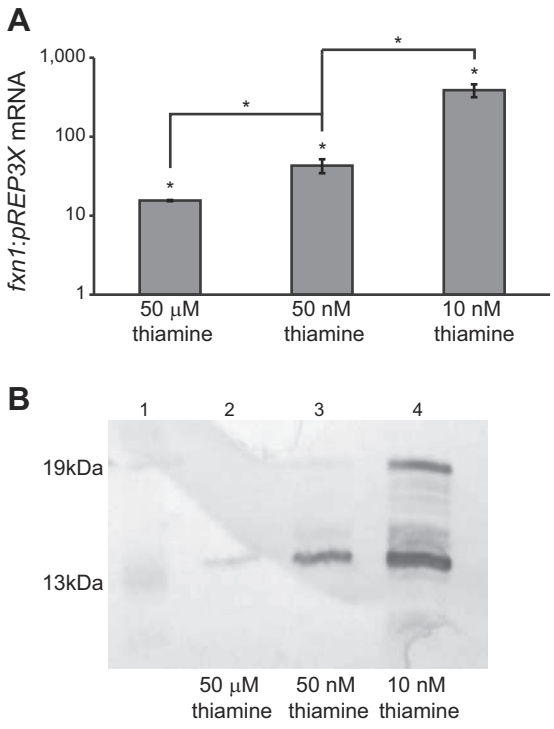

Fig. 2. The Fxn1 overexpression levels and isoforms are controlled by thiamine concentration. (A) *S. pombe* wild-type cells with pREP3X or pREP3X/Fxn1 were grown to mid-log phase with 50 μM, 50 nM or 10 nM thiamine. Total RNA was used as the template for cDNA synthesis and qRT-PCR was performed. The relative *fxn1* mRNA levels were normalized to the α-actin gene [24]. Values are the fold difference compared to pREP3X cells ($n = 3$) with the mean ± S.E.M., where $^*p < 0.05$. (B) SDS-PAGE was run with 10 μg total mitochondrial protein from pREP3X or pREP3X/Fxn1-6His transformants cultured in 10 nM, 50 nM or 50 μM thiamine. After transfer to a membrane a Western blot was performed with an anti-His antibody and alkaline phosphatase staining. Lane 1: ProSieve pre-stained ladder; lane 2: 50 μM thiamine; lane 3: 50 nM thiamine; lane 4: 10 nM thiamine.

Fig. S4), consistent with human frataxin isoforms [54], so the change in electrophoretic mobility on a native gel is most likely due to aggregation/oligomerization of Fxn1 [55].

3.4. Iron metabolism in cells overexpressing Fxn1

Mitochondria are highly involved in iron metabolism and disruption of mitochondrial function often leads to altered whole-cell iron processing [56]. Since frataxin deficiency leads to mitochondrial iron accumulation [33,57], we investigated whether higher concentrations of Fxn1 would yield the opposite effect: a decrease in iron levels. The concentrations of cellular and mitochondrial iron were determined in *S. pombe* pREP3X/Fxn1 transformants grown in minimal media without additional iron (~0.7 μM iron in the media). Surprisingly, cells de-repressed in 10 nM thiamine actually accumulate ~11-fold more cellular iron than control cells (Fig. 3A). The free mitochondrial iron concentration is also elevated up to ~2-fold at the highest level of Fxn1 expression (Fig. 3B). While not directly comparable, the two results show that Fxn1 expression increases iron at the cellular and mitochondrial levels; however, the majority of the accumulated iron is non-mitochondrial.

Iron uptake by *S. pombe* requires reduction of ferric iron (Fe^{3+}) to ferrous iron (Fe^{2+}) by the cell surface enzyme ferrireductase (Frp1), whose activity is up-regulated during iron limitation [58]. Thus, Frp1 activity is a marker of intracellular iron levels, predominantly the bioavailable Fe^{2+} form. The iron-specific chelator bathophenanthrolinedisulfonic acid (BPS) was used as a colorimetric indicator of Frp1 activity since the production of Fe^{2+} can be monitored by the formation of the red Fe^{2+}-BPS complex at the cell surface [43,58]. The enhanced red color of the

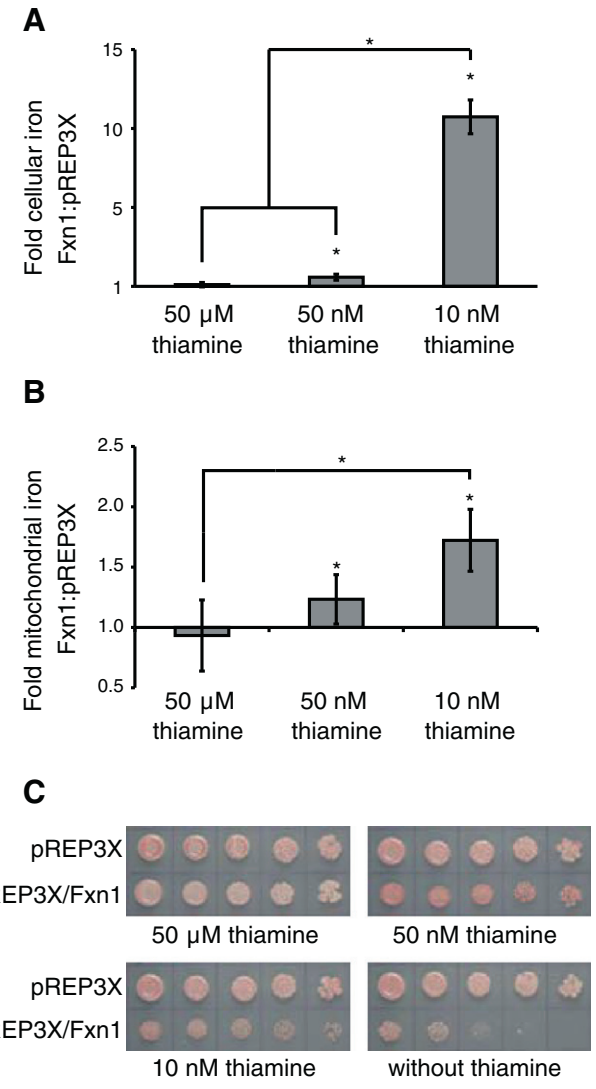

Fig. 3. Overexpression of Fxn1 causes iron accumulation and enhanced ferric reductase activity. pREP3X and pREP3X/Fxn1 transformants were cultured in 50 μM, 50 nM or 10 nM thiamine. (A) The total cellular iron content was measured by BPS and normalized to the number of cells. The fold increase of iron in Fxn1 overexpressing cells was compared to the pREP3X controls. (B) The iron concentrations of mitochondria purified from pREP3X and pREP3X/Fxn1 were measured with BPS and normalized to total protein. Values shown are the fold difference compared to the pREP3X controls. (C) pREP3X and pREP3X/Fxn1 transformants were grown to mid-log phase without thiamine then resuspended to 1×10^7cells/ml. Cells were serially diluted (1:5) and spotted on EMM + AU with 25 μM BPS with 0 nM, 10 nM, 50 nM and 50 μM thiamine. Plates were incubated at 30 °C for 5 days. ($^*p < 0.05$, error bars shown as mean ± S.E.M., $n \geq 5$).

Fe^{2+}-BPS complex is observed for Fxn1 overexpressing transformants compared to the control strains (Fig. 3C). It is especially noticeable at 50 nM thiamine where the growth inhibition is not as severe. Even though increased Fxn1 levels cause iron to accumulate in cells and mitochondria, Frp1 activation indicates that the cell has signaled the need to import iron [33]. This also suggests that the accumulated iron inside the cell may be oxidized Fe^{3+}, which has a low solubility in aqueous solution and may be unavailable for iron metabolism [59].

Because of the iron accumulation, serial dilution growth assays were performed in the presence of cell-impermeable and cell-permeable metal chelators to determine if iron limitation could rescue the growth deficit upon Fxn1 overexpression. Transformants were grown in minimal media with 50 μM thiamine (i.e., fully repressed), then cultured in media without thiamine to express Fxn1. EMM minimal media contains ~0.7 μM iron, so iron was not limiting until cells were plated onto agar

with chelators. All chelators are inhibitory to the growth of pREP3X control cells to varying degrees (Supplementary Fig. S5). Fxn1 overexpression still inhibits growth, but no additional growth inhibition from iron chelation is observed as it is for control cells. The most obvious protective effect is with the combination of the high affinity iron chelator DTPA and the membrane-permeable chelator deferoxamine, which chelates labile intracellular iron [60]. It is possible that the combination of iron-deplete media and cell-permeable iron chelation limits iron uptake and accumulation such that Fxn1 overexpressing cells are more resistant to growth inhibition arising from metal depletion [61]. It also suggests that the accumulation of iron at high levels of Fxn1 is related to the loss of cell viability since the growth can be rescued by iron limitation.

3.5. Effect of Fxn1 overexpression on the activities of mitochondrial Fe–S cluster enzymes

Mitochondrial Fe–S cluster biogenesis provides essential Fe–S cluster cofactors for proteins, and the pathway is responsive to both iron levels and oxidative stress [17,56]. Since Fxn1 overexpressing transformants accumulate 2-fold more iron than control cells, Fe–S cluster synthesis could be affected. The relative activities of two mitochondrial Fe–S cluster enzymes, aconitase and succinate dehydrogenase (SDH), were examined in Fxn1 overexpressing transformants. Aconitase is a tricarboxylic acid (TCA) cycle enzyme [62], while SDH links the respiratory chain to the TCA cycle [47]. Thus, Fe–S cluster synthesis and maturation of Fe–S containing proteins are functionally required for aerobic cell growth [63]. In spite of the inhibited growth of Fxn1 transformants, aconitase activity relative to total mitochondrial protein increases up to ~3.8-fold at all levels of Fxn1 overexpression compared to control cells (i.e., fold increase in relative activity is >1) (Fig. 4A). Averaged aconitase progress curves clearly show that the reaction rate increases as a function of Fxn1 overexpression (Supplementary Fig. S6). Relative SDH activities from cells overexpressing Fxn1 are also statistically higher than the control strains at all thiamine concentrations; however, there was no statistical relevance between the levels of Fxn1 overexpression themselves (Fig. 4B). Quantitative RT-PCR with Fxn1 overexpressing transformants indicate that the increased Fe–S enzyme activities are not due to up-regulated transcription of mitochondrial aconitase (*acon1*) or SDH (*sdh2*) genes (Table 2). Therefore, Fxn1 overexpression in general leads to increased relative aconitase and SDH activities at the protein level, which could be related to the fraction of enzyme with active Fe–S clusters [64].

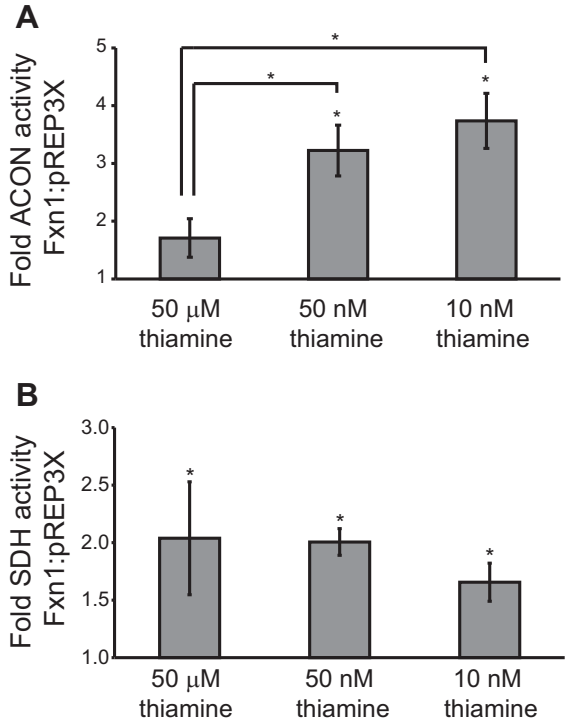

Fig. 4. Mitochondrial aconitase and succinate dehydrogenase relative activities increase in Fxn1 overexpressing cells. Mitochondria were purified from pREP3X and pREP3X/Fxn1 transformants cultured in 50 μM, 50 nM or 10 nM thiamine ($n \geq 5$, error bars are shown as mean ± S.E.M., $^*p < 0.05$). (A) The aconitase (ACON) activity was measured with 12.5 μg of purified mitochondria. The rate was monitored as a change in absorbance at 340 nm and was normalized to the total mitochondrial protein in each reaction. (B) Succinate dehydrogenase (SDH) activity was measured with 100 μg of purified mitochondria. The absorbance change at 600 nm of each reaction after 5 min was normalized to the total amount of protein and plotted as the fold increase in activity compared to control pREP3X cells.

It is possible that genes encoding proteins of the Fe–S cluster biosynthetic complex are up-regulated from the increased iron concentrations in Fxn1 overexpressing cells [59]. The transcriptional levels of the cysteine desulfurase Nfs1, the Fe–S cluster scaffold protein Isu1, and the accessory protein Isd11 were determined by RT-PCR in Fxn1 overexpressing strains (Table 2). No statistically significant changes in transcript level are observed for *nfs1*, while *isu1* and *isd11* transcript levels are both increased in Fxn1 overexpression strains. This suggests that Fxn1 levels may directly or indirectly regulate the transcription of some Fe–S cluster biosynthetic complex proteins, which may lead to increased Fe–S cluster biogenesis.

3.6. Mild Fxn1 overexpression confers cellular resistance to oxidative stress

Since excess iron can produce reactive oxygen species (ROS) [65], growth assays were performed to determine whether Fxn1 overexpressing strains were sensitive to external hydrogen peroxide stress [66]. H_2O_2 decreases the viability of pREP3X control cells, but not those overexpressing low levels of Fxn1 (Fig. 5A). This indicates that slight increases in Fxn1 are protective and increase resistance to oxidative stress. Higher overexpression of Fxn1 (50 and 10 nM thiamine) did not have a protective effect against peroxide stress (data not shown), which is consistent with the growth inhibition observed under these conditions (Fig. 1). It is possible that antioxidant enzymes such as superoxide dismutase (SOD) and catalase contribute to the resistance to external oxidative stress at low Fxn1 levels. Cytosolic (SOD1) and mitochondrial (SOD2) enzymes reduce superoxide anions to hydrogen peroxide, which is further reduced to water by catalase [67]. Total relative SOD activity (SOD1/SOD2) for all Fxn1 overexpressing strains is significantly higher compared to that for control cells (Fig. 5B), but the activity is not correlated with Fxn1 concentration. The levels of *sod1* transcript also increases 1.7-fold for cells cultured in 50 μM and 50 nM thiamine (Table 2). In addition, total relative catalase activity increases over 2-fold for cells overexpressing Fxn1; however, but the activity does not vary significantly with Fxn1 concentration (Fig. 5C). Thus, cells with slight overexpression of Fxn1 have a “pre-induced” oxidative stress response that is consistent with low levels of ROS, but this response is not adequate to overcome the more extensive oxidative stress created at high Fxn1expression levels (Fig. S1).

4. Discussion

The highly conserved protein frataxin, whose deficiency leads to the neurodegenerative disease Friedreich's ataxia (FA), is linked to mitochondrial iron metabolism in eukaryotic cells [57]. The precise biological function of frataxin has been researched in multiple model systems, but is still a matter of debate [12]. This is due, in part, to the conflicting results as to which phenotypes are direct consequences of frataxin deficiency and which are secondary consequences from disrupted of iron homeostasis [28]. One approach to dissect these roles is to overexpress frataxin in a model organism and characterize the phenotypic changes that result. Overexpression of frataxin and homologues has been studied in

Table 2
The relative mRNA levels of specific genes in iron metabolism and oxidative stress.[a]

	50 μM thiamine		50 nM thiamine		10 nM thiamine	
	pREP3X	pREP3X/Fxn1	pREP3X	pREP3X/Fxn1	pREP3X	pREP3X/Fxn1
fxn1	1.00 ± 0.06	15.5 ± 0.26*	1.01 ± 0.07	43 ± 8.5*	1.00 ± 0.05	387 ± 71.9*
acon1	1.00 ± 0.06	0.78 ± 0.05	1.00 ± 0.05	0.95 ± 0.10	1.02 ± 0.13	0.81 ± 0.05
sdh1	1.00 ± 0.04	0.96 ± 0.11	1.01 ± 0.09	1.29 ± 0.05	1.000 ± 0.004	0.72 ± 0.07
sdh2	1.00 ± 0.05	0.82 ± 0.03	1.01 ± 0.12	0.94 ± 0.05	1.00 ± 0.03	0.620 ± 0.007
isu1	1.00 ± 0.06	1.52 ± 0.29*	1.01 ± 0.07	1.34 ± 0.19*	1.00 ± 0.02	1.86 ± 0.46*
nfs1	1.01 ± 0.09	1.2 ± 0.15	1.05 ± 0.23	0.97 ± 0.19	1.00 ± 0.03	1.041 ± 0.012
isd11	1.0 ± 0.1	1.32 ± 0.08*	1.03 ± 0.18	1.27 ± 0.22*	1.01 ± 0.12	0.92 ± 0.04
sod1	1.00 ± 0.05	1.76 ± 0.04*	1.03 ± 0.17	1.70 ± 0.11*	1.00 ± 0.04	1.1 ± 0.2
sod2	1.00 ± 0.07	1.33 ± 0.02	1.0 ± 0.1	0.84 ± 0.02	1.00 ± 0.06	0.95 ± 0.15

[a] Three transformants of pREP3X and pREP3X/Fxn1 were each cultured with 50 μM, 50 nM or 10 nM thiamine for 72 h at 30 °C. The primers for genes assayed by quantitative real time PCR are in Table S1 in the Supplementary data. The relative expression levels were calculated using the actin *act1* housekeeping gene [24]. Three technical replicates were averaged for each biological replicate and reported as mean ± S.E.M. (*$p < 0.05$).

S. cerevisiae, mouse, fly, and human cell lines, but these studies have produced contradictory results [26–30,68–71]. As listed in Table 1, overexpression of human frataxin in human cell lines and mouse models indicates that increased frataxin concentrations enhance both cellular respiration and relative aconitase activity (or oxidative phosphorylation) [68,70,72]. However, fly and yeast studies observed decreased aconitase relative activity and impaired cellular respiration if frataxin was overexpressed [28,29]. The reason for these discrepancies is unclear, but may be related to the level of frataxin overexpression, which is the focus of this study using *Schizosaccharomyces pombe* as a model organism. *S. pombe* fission yeast is an attractive model organism for human mitochondrial diseases such as FA as it is a unicellular eukaryote that is evolutionarily distant from *S. cerevisiae* and a good organism to study mitochondrial diseases [31,73]. The *S. pombe* frataxin homologue Fxn1 (also called Pfh1) is 44% identical to human frataxin and is known to closely replicate the FA phenotype upon its deletion (*fxn1*Δ) [33]. For these reasons we characterized the phenotypic effects of *S. pombe* Fxn1 overexpression, providing a complementary way to investigate the function of frataxin. Our characterization has also shed light onto the reason for the inconsistencies in other frataxin overexpression models.

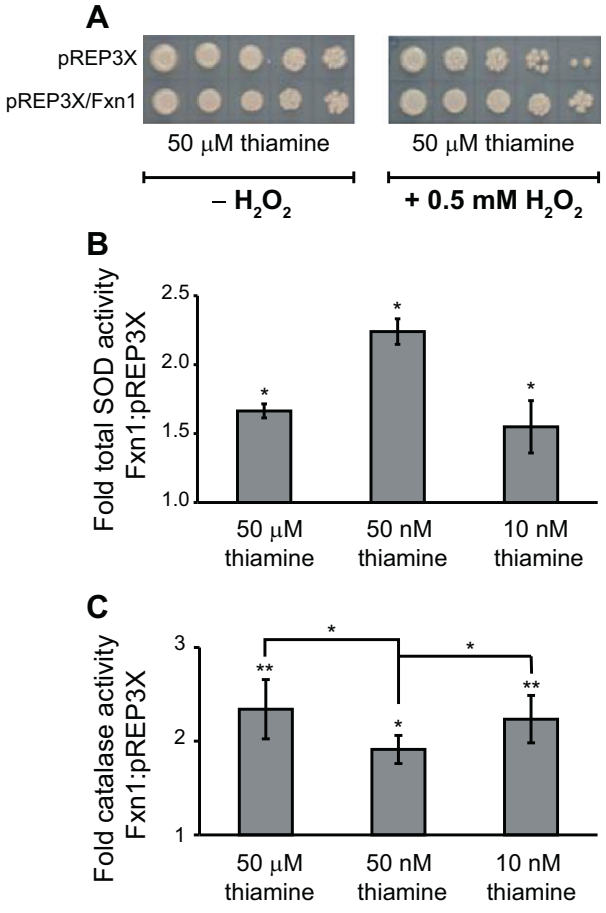

Fig. 5. Fxn1 overexpression induces a cellular response to oxidative stress. (A) pREP3X and pREP3X/Fxn1 transformants were grown to mid-log phase without thiamine then resuspended to 1×10^7cells/ml. Cells were serially diluted on agar containing 0.5 mM H_2O_2 and either 10 nM, 50 nM and 50 μM thiamine. Only 50 μM thiamine is shown. (B) Relative superoxide (SOD) activity was measured with 5 μg of cell lysate from pREP3X and pREP3X/Fxn1 transformants cultured in 50 μM, 50 nM or 10 nM thiamine. Activities were normalized to the total protein concentration and plotted as the fold difference of Fxn1 cells compared to control pREP3X cells ($n \geq 4$, error bars are shown as S.E.M., *, $p < 0.05$). (C) Relative catalase activity was measured with 2 μg of cell lysate from pREP3X and pREP3X/Fxn1 transformants cultured in 50 μM, 50 nM or 10 nM thiamine. Activities were normalized to the total protein concentration and plotted as the fold difference of Fxn1 cells compared to control pREP3X cells ($n \geq 4$, error bars are shown as mean ± S.E.M., *$p < 0.05$, **$p < 0.01$).

The expression of exogenous *S. pombe* Fxn1 was controlled via a thiamine-repressible promoter [34,35]. Three Fxn1 expression levels over native amounts were compared: high (~380-fold), moderate (~40-fold) and low (~15-fold) overexpression corresponding to 10 nM, 50 nM and 50 μM thiamine, respectively (Fig. 2A). The "low-moderate" (50 μM and 50 nM thiamine) and "high" (10 and 0 nM thiamine) Fxn1 overexpression phenotypes are distinct and summarized in Table 3.

Mature *S. pombe* Fxn1 is composed of residues 38–158 (Fig. S2) and is the major isoform in cells with low–moderate overexpression (Fig. 2B). The full-length ~19 kDa Fxn1 isoform was observed at high overexpression levels (Fig. 2B), along with protein oligomerization/aggregation (Fig. S3). Under aerobic conditions, cell viability declined for both the low-moderate and high overexpression phenotypes (Fig. 1A); however, high Fxn1 levels caused severe growth inhibition that was not from general mitochondrial protein overexpression as this level of inhibition was not observed for the Fe–S scaffold Isu1 (Fig. 1B) or in other *S. pombe* overexpression studies [74,75]. We propose that the degree of growth inhibition from Fxn1 expression is related to the amount of unprocessed Fxn1 or to the amount of frataxin in oligomeric complexes, similar to Yfh1 [48]. Contradictory studies indicating frataxin oligomerization is functional [76,77] and not non-functional [78] have been reported, so a more detailed examination is required in *S. pombe*.

Similar to other *S. pombe* mutants with mitochondrial dysfunction [79], cells with high Fxn1 overexpression exhibited clear morphological and mitochondrial membrane abnormalities (Fig. 1C) and were respiratory-deficient, unlike the low-moderate overexpressing cells which had slightly increased cellular respiration (Fig. 1F). The *S. pombe fxn1*Δ strain also had a decreased respiration rate [33], so it is interesting that mitochondrial dysfunction appears to be related to both Fxn1 deficiency and high mitochondrial Fxn1 overexpression, but not at low-moderate levels. Further studies indicated that oxidative stress, a

Table 3
Summary of *S. pombe* Fxn1 overexpression phenotypes.

Property	Low–moderate overexpression (14 – 40 fold)[a]	High overexpression (380 fold)[a]
Cell growth (aerobic)	Slightly inhibited	Severely inhibited
Cell growth (anaerobic)	No difference compared to aerobic	Less inhibited compared to aerobic
Cell morphology	Few bottle shaped	Majority bottle shaped
Mitochondrial membrane integrity	Some aggregation at 50 nM	Severely aggregated/fragmented
Cell respiration rate	Increased ~20% of control	Decreased ~80% of control
Isoform	$Fxn1^{38–158}$	$FXN1^{38–158}$ and $FXN1^{1–158}$
Fxn1 aggregation	No	Yes
Cellular iron accumulation	Slight increase	Increased ~11-fold
Mitochondrial iron accumulation	No significant increase	Increased ~2-fold
Growth with Fe chelators	Less inhibition than control	Less inhibition than control
Oxidative stress	Slight increase	Significant increase
Induced ROS response	Yes	Yes
SDH activity	Increased ~2-fold	Increased ~2-fold
Aconitase activity	Increased 1.8–3.2-fold	Increased ~4-fold
SOD activity	Increased 1.7–2.3-fold	Increased ~1.5-fold
Catalase activity	Increased 1.9–2.3-fold	Increased 2.3-fold
Growth with external ROS	Growth enhanced compared to control	No difference

[a] Determined from quantitative RT-PCR of *fxn1* gene.

hallmark of respiratory deficiency [80], may play a role in this dysfunction in the high overexpression phenotype [67]. Although ROS is likely present in both Fxn1 overexpression phenotypes, it is more severe at the highest Fxn1 levels. Low amounts of Fxn1 up-regulated SOD and catalase activities to actually protect *S. pombe* from external peroxide stress (Fig. 5A); however, the ROS correlated with the high expression phenotype presumably exceeds the antioxidant capacity, leading to loss of cellular viability. Cell viability was somewhat restored under anaerobic conditions, which bypasses the aerobic respiratory chain (Fig. 1A). Anaerobic growth also rescued the *fxn1Δ S. pombe* strain, which had clear markers of ROS [33]. Therefore, we propose that the growth inhibition of *S. pombe* cells overexpressing high levels of Fxn1 is from mitochondrial dysfunction and/or oxidative stress.

The 11-fold cellular and 2-fold mitochondrial accumulation of iron in the high Fxn1 overexpression phenotype levels suggested that dysregulated iron metabolism may contribute to oxidative stress and growth inhibition of *S. pombe* cells (Fig. 3A), although further investigation into the type of ROS present is required to confirm this prediction [30,48]. Extra- and intra-cellular iron chelators improved cell viability of Fxn1 overexpressing cells, providing further support for the link between excess iron and cell growth (Supplementary Fig. S5). Even moderate Fxn1 concentrations led to increased ferric reductase activity at the cell surface (Fig. 3C), which is part of the high affinity iron uptake pathway that is up-regulated by iron limitation [30,58]. Potential induction of the "iron-deficient" cellular response suggests that some of the accumulated iron in the high overexpression phenotype may be non-labile (e.g., in ferric aggregates or nanoparticles) [33,81]; however, more studies are required to confirm the oxidation state and chemical species of the accumulated iron. Further, mitochondrial iron accumulation in frataxin-deficient cells is known to be proportional to the amount of iron in the media [82]. Therefore, it is difficult to compare the levels of iron accumulation in our studies which did not supplement growth media with iron (i.e., 0.7 μM) to the many studies of frataxin-deficiency that added iron to the culture media. In Yfh1-deficient yeast, a relative depletion in cytosolic iron accompanies the increase in mitochondrial iron [20], and reintroduction of exogenous Yfh1 (5-fold overexpression) appears to redistribute iron from the mitochondria to the cytosol [18]. These results are similar to our observations with *S. pombe* Fxn1 overexpression, where most accumulated iron is in the cytosol. This is not to say that the small increase in mitochondrial iron from Fxn1 overexpression is not without consequence. Some researchers postulate that significant iron accumulation may be a late event in FA, but subtle increases in mitochondrial iron levels may be an early event and may play a role in the pathogenesis of FA (i.e., Fe–S cluster deficits and oxidative stress) [18,83]. In fact, our iron accumulation data are actually more consistent with mammalian FA models with frataxin-depletion or deficiency in which mitochondrial iron only increases 1.5–3 fold [84,85], as compared to 2–12 fold for *S. cerevisiae yfh1Δ* knockout strains [18]. This is another reason *S. pombe* is an attractive model for FA studies.

The accumulated mitochondrial iron from Fxn1 overexpression was likely shunted to Fe–S cluster biogenesis in some way. *S. pombe* aconitase and succinate dehydrogenase (SDH) enzymes both require intact Fe–S clusters for activity [48,56]. Aconitase activity normalized to total protein increased for both Fxn1 overexpression phenotypes (Fig. 4A) and was not due to increased *acon1* transcription (Table 2). Relative SDH activity was also enhanced for both the low-moderate and high Fxn1 overexpression phenotypes; however, there was no statistical relationship between activity and amount of Fxn1 (Fig. 4B). Given that both aconitase and SDH displayed increased normalized activities, it is likely that Fxn1 overexpression stimulates Fe–S cluster synthesis or maturation of Fe–S proteins using some of the imported mitochondrial iron.

Mitochondrial Fe–S clusters are synthesized on the Isu1 scaffold protein using sulfur from the cysteine desulfurase Nfs1 in complex with an accessory protein Isd11 [56]. Frataxin may donate iron for Fe–S cluster assembly, although recent experiments suggest that frataxin regulates Nfs1 cysteine desulfurase activity and sulfur mobilization for Fe–S biogenesis [15,16]. If Fxn1 regulates the production of Fe–S clusters, overexpression of Fxn1 would activate Fe–S cluster biosynthesis, leading to increased maturation of Fe–S containing proteins like aconitase and SDH. We determined that *nfs1* and *isd11* transcript levels were not greatly altered by Fxn1 overexpression (Table 2); however, *isu1* transcription, which is regulated by mitochondrial iron availability [86], was increased for both low-moderate and high Fxn1 overexpression phenotypes. As a result, it is possible that activation of Fe–S biosynthesis by Fxn1 could lead to up-regulated *isu1* transcription and increased iron import to support cluster production [63]. This is a very interesting avenue for future investigations of Fxn1 function during Fe–S biogenesis.

Finally, the augmented normalized aconitase activity in *S. pombe* Fxn1 overexpressing cells is interesting from a functional standpoint since the catalytic [4Fe–4S] cluster is sensitive to oxidative damage and enzyme inactivation [87]. Our studies suggest that cells overexpressing Fxn1 experience some level of oxidative stress, so it is unusual that aconitase activity was enhanced, but not without support in the literature. Other frataxin overexpression studies in mouse [26], human adipocytes [68], and human cancer cells [70] also reported increased aconitase activities (Table 2). None of these studies presented a hypothesis for increased aconitase activity in relation to Fxn1. Frataxin overexpression in *S. cerevisiae* [28] or *Drosophila* [71] actually led to a decline in aconitase activity. This could indicate that *S. pombe* Fxn1 has functions more conserved with mammalian frataxin than

S. cerevisiae and *Drosophila* orthologues, which supports its use as a model organism for FA research [42]. The increased aconitase activity detected in Fxn1 overexpressing *S. pombe* cells is also consistent with a study by Bulteau *et al.* that demonstrated that the Fe–S cluster in *S. cerevisiae* aconitase is protected from oxidation through a direct interaction with Yfh1 [19]. A more likely scenario is that oxidatively damaged Fe–S clusters undergo faster turnover using imported mitochondrial iron. This would not be as noticeable for SDH as its Fe–S clusters are not as sensitive to oxidative stress [47].

5. Conclusions

S. pombe cells overexpressing Fxn1 have two phenotypes distinguished by the amount of Fxn1 in the mitochondria. It appears as though low-to-moderate overproduction of Fxn1 may lead to some beneficial effects, whereas the significant overexpression of Fxn1 over some threshold value may be toxic to the overall health of the cell. These two phenotypes also potentially explain the phenotypic discrepancies between overexpression studies in other organisms (Table 2). This study indicates that Fxn1 protein levels must be balanced to properly carry out its role in Fe–S cluster biogenesis. We propose that since activated Fe–S cluster synthesis or maturation is common to both phenotypes, Fxn1 may be a regulator for this process as proposed for other frataxin homologues [15,16]. Enhanced production of Fe–S clusters at low-moderate Fxn1 concentrations explains the slightly stimulated cellular respiration rate and iron uptake. Any unused iron could undergo redox chemistry with oxygen and contribute to low level oxidative stress that up-regulates antioxidant enzymes like SOD and catalase [67]. At high Fxn1 overexpression levels, cells continue to import iron to their detriment. Since the cell is presumably replete in Fe–S clusters, the decreased cellular respiration, mitochondrial fragmentation, and inhibition of cell growth observed at high Fxn1 levels may be due to iron-based oxidative stress, not Fe–S cluster deficits in electron transport chain proteins [48]. Despite its known sensitivity to oxidative stress, aconitase activity was enhanced under these cellular conditions, which further supports the hypothesis that Fe–S cluster production has been up-regulated by Fxn1, although other potential mechanisms of oxidative stress must also be explored [88].

Based on the prediction that Fxn1 is an activator of Fe–S synthesis [15,16], its deficiency in FA would clearly decrease Fe–S cluster biogenesis and downstream activities of Fe–S-containing proteins including aconitase, SDH, and some in the electron transport chain. In this case, oxidative stress would be created through a feedback-loop mechanism related to respiratory deficiency and iron accumulation [48]. These phenotypes have been observed as hallmarks of Friedreich's ataxia: respiratory deficit, decreased activities of Fe–S enzymes, mitochondrial iron accumulation and oxidative stress [3]. Deletion of *S. pombe fxn1* reproduces the FA phenotype [33] and Fxn1 overexpression delineates a regulatory role in Fe–S cluster biosynthesis. This would suggest that dysregulation of Fe–S cluster biogenesis is involved in the pathogenesis of Friedreich's ataxia. Putting our research in context with other studies, it also suggests that therapies to increase transcription and translation of endogenous frataxin or to replace exogenous frataxin via gene therapy must tightly control protein expression since high levels of frataxin are detrimental to the cell in a manner similar to its deficiency [26–30, 68–71].

Acknowledgements

This material is based upon work supported by the National Science Foundation under Grant Number MCB #0845273 (to L.S.B.). We thank Dr. Brittney McInnis and Huan Li for their technical assistance with microscopy experiments, Prof. Marco Bonizzoni (Department of Chemistry) for the use of his plate reader, and Prof. Matthew Jenny (Department of Biological Sciences) for technical assistance and use of the real time thermocycler.

Appendix A. Supplementary data

Supplementary data to this article can be found online at http://dx.doi.org/10.1016/j.bbagen.2014.06.017.

References

[1] M. Cossee, M. Schmitt, V. Campuzano, L. Reutenauer, C. Moutou, J.L. Mandel, M. Koenig, Evolution of the Friedreich's ataxia trinucleotide repeat expansion: founder effect and premutations, Proc. Natl. Acad. Sci. U. S. A. 94 (1997) 7452–7457.
[2] D. Marmolino, Friedreich's ataxia: past, present and future, Brain Res. Rev. 67 (2011) 311–330.
[3] A. Rotig, P. de Lonlay, D. Chretien, F. Foury, M. Koenig, D. Sidi, A. Munnich, P. Rustin, Aconitase and mitochondrial iron-sulphur protein deficiency in Friedreich ataxia, Nat. Genet. 17 (1997) 215–217.
[4] V. Campuzano, L. Montermini, M.D. Molto, L. Pianese, M. Cossee, F. Cavalcanti, E. Monros, F. Rodius, F. Duclos, A. Monticelli, F. Zara, J. Canizares, H. Koutnikova, S.I. Bidichandani, C. Gellera, A. Brice, P. Trouillas, G. De Michele, A. Filla, R. De Frutos, F. Palau, P.I. Patel, S. Di Donato, J.L. Mandel, S. Cocozza, M. Koenig, M. Pandolfo, Friedreich's ataxia: autosomal recessive disease caused by an intronic GAA triplet repeat expansion, Science 271 (1996) 1423–1427.
[5] K. Ohshima, L. Montermini, R.D. Wells, M. Pandolfo, Inhibitory effects of expanded GAA.TTC triplet repeats from intron I of the Friedreich ataxia gene on transcription and replication in vivo, J. Biol. Chem. 273 (1998) 14588–14595.
[6] H.L. Plasterer, E.C. Deutsch, M. Belmonte, E. Egan, D.R. Lynch, J.R. Rusche, Development of frataxin gene expression measures for the evaluation of experimental treatments in Friedreich's ataxia, PLoS One 8 (2013) e63958.
[7] G. Musco, G. Stier, B. Kolmerer, S. Adinolfi, S. Martin, T. Frenkiel, T. Gibson, A. Pastore, Towards a structural understanding of Friedreich's ataxia: the solution structure of frataxin, Structure 8 (2000) 695–707.
[8] Y. He, S.L. Alam, S.V. Proteasa, Y. Zhang, E. Lesuisse, A. Dancis, T.L. Stemmler, Yeast frataxin solution structure, iron binding, and ferrochelatase interaction, Biochemistry 43 (2004) 16254–16262.
[9] M. Nair, S. Adinolfi, C. Pastore, G. Kelly, P. Temussi, A. Pastore, Solution structure of the bacterial frataxin ortholog, CyaY: mapping the iron binding sites, Structure 12 (2004) 2037–2048.
[10] H. Puccio, D. Simon, M. Cossee, P. Criqui-Filipe, F. Tiziano, J. Melki, C. Hindelang, R. Matyas, P. Rustin, M. Koenig, Mouse models for Friedreich ataxia exhibit cardiomyopathy, sensory nerve defect and Fe–S enzyme deficiency followed by intramitochondrial iron deposits, Nat. Genet. 27 (2001) 181–186.
[11] M.A. Huynen, B. Snel, P. Bork, T.J. Gibson, The phylogenetic distribution of frataxin indicates a role in iron–sulfur cluster protein assembly, Hum. Mol. Genet. 10 (2001) 2463–2468.
[12] A. Martelli, M. Napierala, H. Puccio, Understanding the genetic and molecular pathogenesis of Friedreich's ataxia through animal and cellular models, Dis. Model. Mech. 5 (2012) 165–176.
[13] T. Yoon, J.A. Cowan, Iron–sulfur cluster biosynthesis. Characterization of frataxin as an iron donor for assembly of [2Fe-2S] clusters in ISU-type proteins, J. Am. Chem. Soc. 125 (2003) 6078–6084.
[14] G. Layer, S. Ollagnier-de Choudens, Y. Sanakis, M. Fontecave, Iron–sulfur cluster biosynthesis: characterization of Escherichia coli CyaY as an iron donor for the assembly of [2Fe-2S] clusters in the scaffold IscU, J. Biol. Chem. 281 (2006) 16256–16263.
[15] C.L. Tsai, D.P. Barondeau, Human frataxin is an allosteric switch that activates the Fe–S cluster biosynthetic complex, Biochemistry 49 (2010) 9132–9139.
[16] F. Colin, A. Martelli, M. Clemancey, J.M. Latour, S. Gambarelli, L. Zeppieri, C. Birck, A. Page, H. Puccio, S. Ollagnier de Choudens, Mammalian frataxin controls sulfur production and iron entry during de novo Fe(4)S(4) cluster assembly, J. Am. Chem. Soc. 135 (2013) 733–740.
[17] O.S. Chen, S. Hemenway, J. Kaplan, Inhibition of Fe–S cluster biosynthesis decreases mitochondrial iron export: evidence that Yfh1p affects Fe–S cluster synthesis, Proc. Natl. Acad. Sci. U. S. A. 99 (2002) 12321–12326.
[18] U. Muhlenhoff, N. Richhardt, M. Ristow, G. Kispal, R. Lill, The yeast frataxin homolog Yfh1p plays a specific role in the maturation of cellular Fe/S proteins, Hum. Mol. Genet. 11 (2002) 2025–2036.
[19] A.L. Bulteau, H.A. O'Neill, M.C. Kennedy, M. Ikeda-Saito, G. Isaya, L.I. Szweda, Frataxin acts as an iron chaperone protein to modulate mitochondrial aconitase activity, Science 305 (2004) 242–245.
[20] F. Foury, O. Cazzalini, Deletion of the yeast homologue of the human gene associated with Friedreich's ataxia elicits iron accumulation in mitochondria, FEBS Lett. 411 (1997) 373–377.
[21] T. Yoon, J.A. Cowan, Frataxin-mediated iron delivery to ferrochelatase in the final step of heme biosynthesis, J. Biol. Chem. 279 (2004) 25943–25946.
[22] M. Cossee, H. Puccio, A. Gansmuller, H. Koutnikova, A. Dierich, M. LeMeur, K. Fischbeck, P. Dolle, M. Koenig, Inactivation of the Friedreich ataxia mouse gene leads to early embryonic lethality without iron accumulation, Hum. Mol. Genet. 9 (2000) 1219–1226.
[23] C.J. Miranda, M.M. Santos, K. Ohshima, J. Smith, L. Li, M. Bunting, M. Cossee, M. Koenig, J. Sequeiros, J. Kaplan, M. Pandolfo, Frataxin knockin mouse, FEBS Lett. 512 (2002) 291–297.
[24] P.R. Anderson, K. Kirby, A.J. Hilliker, J.P. Phillips, RNAi-mediated suppression of the mitochondrial iron chaperone, frataxin, in Drosophila, Hum. Mol. Genet. 14 (2005) 3397–3405.
[25] A.D. Sheftel, A.B. Mason, P. Ponka, The long history of iron in the universe and in health and disease, Biochim. Biophys. Acta 1820 (2011) 161–187.

[26] C.J. Miranda, M.M. Santos, K. Ohshima, M. Tessaro, J. Sequeiros, M. Pandolfo, Frataxin overexpressing mice, FEBS Lett. 572 (2004) 281–288.
[27] A.P. Runko, A.J. Griswold, K.T. Min, Overexpression of frataxin in the mitochondria increases resistance to oxidative stress and extends lifespan in Drosophila, FEBS Lett. 582 (2008) 715–719.
[28] A. Seguin, A. Bayot, A. Dancis, A. Rogowska-Wrzesinska, F. Auchere, J.M. Camadro, A. L. Bulteau, E. Lesuisse, Overexpression of the yeast frataxin homolog (Yfh1): contrasting effects on iron–sulfur cluster assembly, heme synthesis and resistance to oxidative stress, Mitochondrion 9 (2009) 130–138.
[29] J.A. Navarro, J.V. Llorens, S. Soriano, J.A. Botella, S. Schneuwly, M.J. Martinez-Sebastian, M.D. Molto, Overexpression of human and fly frataxins in Drosophila provokes deleterious effects at biochemical, physiological and developmental levels, PLoS One 6 (2011) e21017.
[30] C.D. Kaplan, J. Kaplan, Iron acquisition and transcriptional regulation, Chem. Rev. 109 (2009) 4536–4552.
[31] L. Aravind, H. Watanabe, D.J. Lipman, E.V. Koonin, Lineage-specific loss and divergence of functionally linked genes in eukaryotes, Proc. Natl. Acad. Sci. U. S. A. 97 (2000) 11319–11324.
[32] V. Wood, R. Gwilliam, M.A. Rajandream, M. Lyne, R. Lyne, A. Stewart, J. Sgouros, N. Peat, J. Hayles, S. Baker, D. Basham, S. Bowman, K. Brooks, D. Brown, S. Brown, T. Chillingworth, C. Churcher, M. Collins, R. Connor, A. Cronin, P. Davis, T. Feltwell, A. Fraser, S. Gentles, A. Goble, N. Hamlin, D. Harris, J. Hidalgo, G. Hodgson, S. Holroyd, T. Hornsby, S. Howarth, E.J. Huckle, S. Hunt, K. Jagels, K. James, L. Jones, M. Jones, S. Leather, S. McDonald, J. McLean, P. Mooney, S. Moule, K. Mungall, L. Murphy, D. Niblett, C. Odell, K. Oliver, S. O'Neil, D. Pearson, M.A. Quail, E. Rabbinowitsch, K. Rutherford, S. Rutter, D. Saunders, K. Seeger, S. Sharp, J. Skelton, M. Simmonds, R. Squares, S. Squares, K. Stevens, K. Taylor, R.G. Taylor, A. Tivey, S. Walsh, T. Warren, S. Whitehead, J. Woodward, G. Volckaert, R. Aert, J. Robben, B. Grymonprez, I. Weltjens, E. Vanstreels, M. Rieger, M. Schafer, S. Muller-Auer, C. Gabel, M. Fuchs, A. Dusterhoft, C. Fritzc, E. Holzer, D. Moestl, H. Hilbert, K. Borzym, I. Langer, A. Beck, H. Lehrach, R. Reinhardt, T.M. Pohl, P. Eger, W. Zimmermann, H. Wedler, R. Wambutt, B. Purnelle, A. Goffeau, E. Cadieu, S. Dreano, S. Gloux, V. Lelaure, S. Mottier, F. Galibert, S.J. Aves, Z. Xiang, C. Hunt, K. Moore, S.M. Hurst, M. Lucas, M. Rochet, C. Gaillardin, V.A. Tallada, A. Garzon, G. Thode, R.R. Daga, L. Cruzado, J. Jimenez, M. Sanchez, F. del Rey, J. Benito, A. Dominguez, J.L. Revuelta, S. Moreno, J. Armstrong, S.L. Forsburg, L. Cerutti, T. Lowe, W.R. McCombie, I. Paulsen, J. Potashkin, G.V. Shpakovski, D. Ussery, B.G. Barrell, P. Nurse, The genome sequence of Schizosaccharomyces pombe, Nature 415 (2002) 871–880.
[33] N. Gabrielli, J. Ayte, E. Hidalgo, Cells lacking pfh1, a fission yeast homolog of mammalian frataxin protein, display constitutive activation of the iron starvation response, J. Biol. Chem. 287 (2012) 43042–43051.
[34] S.L. Forsburg, Comparison of Schizosaccharomyces pombe expression systems, Nucleic Acids Res. 21 (1993) 2955–2956.
[35] K. Maundrell, nmt1 of fission yeast. A highly transcribed gene completely repressed by thiamine, J. Biol. Chem. 265 (1990) 10857–10864.
[36] S. Schmucker, A. Martelli, F. Colin, A. Page, M. Wattenhofer-Donze, L. Reutenauer, H. Puccio, Mammalian frataxin: an essential function for cellular viability through an interaction with a preformed ISCU/NFS1/ISD11 iron–sulfur assembly complex, PLoS One 6 (2011) e16199.
[37] C. Alfa, P. Fantes, J. Hyams, M. McLeod, E. Warbrick, Experiments with Fission Yeast: A Laboratory Course Manual, Cold Spring Harbor Laboratory Press, NY, 1993.
[38] J.P. Javerzat, G. Cranston, R.C. Allshire, Fission yeast genes which disrupt mitotic chromosome segregation when overexpressed, Nucleic Acids Res. 24 (1996) 4676–4683.
[39] Y. Wang, G. Gulis, S. Buckner, P.C. Johnson, D. Sullivan, L. Busenlehner, S. Marcus, The MAP kinase Pmk1 and protein kinase A are required for rotenone resistance in the fission yeast, Schizosaccharomyces pombe, Biochem. Biophys. Res. Commun. 399 (2010) 123–128.
[40] K. Takeda, T. Yoshida, S. Kikuchi, K. Nagao, A. Kokubu, T. Pluskal, A. Villar-Briones, T. Nakamura, M. Yanagida, Synergistic roles of the proteasome and autophagy for mitochondrial maintenance and chronological lifespan in fission yeast, Proc. Natl. Acad. Sci. U. S. A. 107 (2010) 3540–3545.
[41] K.J. Livak, T.D. Schmittgen, Analysis of relative gene expression data using real-time quantitative PCR and the 2(-Delta Delta C(T)) Method, Methods 25 (2001) 402–408.
[42] S. Chiron, M. Gaisne, E. Guillou, P. Belenguer, G.D. Clark-Walker, N. Bonnefoy, Studying mitochondria in an attractive model: Schizosaccharomyces pombe, Methods Mol. Biol. 372 (2007) 91–105.
[43] J. Tamarit, V. Irazusta, A. Moreno-Cermeno, J. Ros, Colorimetric assay for the quantitation of iron in yeast, Anal. Biochem. 351 (2006) 149–151.
[44] A.J. Pierik, D.J. Netz, R. Lill, Analysis of iron–sulfur protein maturation in eukaryotes, Nat. Protoc. 4 (2009) 753–766.
[45] B.A. Ackrell, E.B. Kearney, T.P. Singer, Mammalian succinate dehydrogenase, Methods Enzymol. 53 (1978) 466–483.
[46] V. Worsfold, M.J. Marshall, E.B. Ellis, Enzyme detection using phenazine methosulphate and tetrazolium salts: interference by oxygen, Anal. Biochem. 79 (1977) 152–156.
[47] L. Hederstedt, L. Rutberg, Succinate dehydrogenase–a comparative review, Microbiol. Rev. 45 (1981) 542–555.
[48] R.A. Vaubel, G. Isaya, Iron–sulfur cluster synthesis, iron homeostasis and oxidative stress in Friedreich ataxia, Mol. Cell. Neurosci. 55 (2013) 50–61.
[49] M.J. Barsoum, H. Yuan, A.A. Gerencser, G. Liot, Y. Kushnareva, S. Graber, I. Kovacs, W.D. Lee, J. Waggoner, J. Cui, A.D. White, B. Bossy, J.C. Martinou, R.J. Youle, S.A. Lipton, M.H. Ellisman, G.A. Perkins, E. Bossy-Wetzel, Nitric oxide-induced mitochondrial fission is regulated by dynamin-related GTPases in neurons, EMBO J. 25 (2006) 3900–3911.
[50] A.A. Amchenkova, L.E. Bakeeva, Y.S. Chentsov, V.P. Skulachev, D.B. Zorov, Coupling membranes as energy-transmitting cables. I. Filamentous mitochondria in fibroblasts and mitochondrial clusters in cardiomyocytes, J. Cell Biol. 107 (1988) 481–495.
[51] S. Chiron, A. Bobkova, H. Zhou, M.P. Yaffe, CLASP regulates mitochondrial distribution in Schizosaccharomyces pombe, J. Cell Biol. 182 (2008) 41–49.
[52] S. Lefevre, D. Sliwa, P. Rustin, J.M. Camadro, R. Santos, Oxidative stress induces mitochondrial fragmentation in frataxin-deficient cells, Biochem. Biophys. Res. Commun. 418 (2012) 336–341.
[53] K.M. Robinson, M.S. Janes, M. Pehar, J.S. Monette, M.F. Ross, T.M. Hagen, M.P. Murphy, J.S. Beckman, Selective fluorescent imaging of superoxide in vivo using ethidium-based probes, Proc. Natl. Acad. Sci. U. S. A. 103 (2006) 15038–15043.
[54] S. Schmucker, M. Argentini, N. Carelle-Calmels, A. Martelli, H. Puccio, The in vivo mitochondrial two-step maturation of human frataxin, Hum. Mol. Genet. 17 (2008) 3521–3531.
[55] J. Adamec, F. Rusnak, W.G. Owen, S. Naylor, L.M. Benson, A.M. Gacy, G. Isaya, Iron-dependent self-assembly of recombinant yeast frataxin: implications for Friedreich ataxia, Am. J. Hum. Genet. 67 (2000) 549–562.
[56] R. Lill, B. Hoffmann, S. Molik, A.J. Pierik, N. Rietzschel, O. Stehling, M.A. Uzarska, H. Webert, C. Wilbrecht, U. Muhlenhoff, The role of mitochondria in cellular iron–sulfur protein biogenesis and iron metabolism, Biochim. Biophys. Acta 1823 (2012) 1491–1508.
[57] M. Babcock, D. de Silva, R. Oaks, S. Davis-Kaplan, S. Jiralerspong, L. Montermini, M. Pandolfo, J. Kaplan, Regulation of mitochondrial iron accumulation by Yfh1p, a putative homolog of frataxin, Science 276 (1997) 1709–1712.
[58] D.G. Roman, A. Dancis, G.J. Anderson, R.D. Klausner, The fission yeast ferric reductase gene frp1+ is required for ferric iron uptake and encodes a protein that is homologous to the gp91-phox subunit of the human NADPH phagocyte oxidoreductase, Mol. Cell. Biol. 13 (1993) 4342–4350.
[59] S. Labbe, B. Pelletier, A. Mercier, Iron homeostasis in the fission yeast Schizosaccharomyces pombe, Biometals 20 (2007) 523–537.
[60] E.E. Voest, G. Vreugdenhil, J.J. Marx, Iron-chelating agents in non-iron overload conditions, Ann. Intern. Med. 120 (1994) 490–499.
[61] M. Shakoury-Elizeh, O. Protchenko, A. Berger, J. Cox, K. Gable, T.M. Dunn, W.A. Prinz, M. Bard, C.C. Philpott, Metabolic response to iron deficiency in Saccharomyces cerevisiae, J. Biol. Chem. 285 (2010) 14823–14833.
[62] P.R. Gardner, Aconitase: sensitive target and measure of superoxide, Methods Enzymol. 349 (2002) 9–23.
[63] A. Sheftel, O. Stehling, R. Lill, Iron–sulfur proteins in health and disease, Trends Endocrinol. Metab. 21 (2010) 302–314.
[64] G. Gille, H. Reichmann, Iron-dependent functions of mitochondria–relation to neurodegeneration, J. Neural Transm. 118 (2011) 349–359.
[65] P. Aisen, C. Enns, M. Wessling-Resnick, Chemistry and biology of eukaryotic iron metabolism, Int. J. Biochem. Cell Biol. 33 (2001) 940–959.
[66] L.A. Baker, B.M. Ueberheide, S. Dewell, B.T. Chait, D. Zheng, C.D. Allis, The yeast snt2 protein coordinates the transcriptional response to hydrogen peroxide-mediated oxidative stress, Mol. Cell. Biol. 33 (2013) 3735–3748.
[67] E. Herrero, J. Ros, G. Belli, E. Cabiscol, Redox control and oxidative stress in yeast cells, Biochim. Biophys. Acta 1780 (2008) 1217–1235.
[68] M. Ristow, M.F. Pfister, A.J. Yee, M. Schubert, L. Michael, C.Y. Zhang, K. Ueki, M.D. Michael II, B.B. Lowell, C.R. Kahn, Frataxin activates mitochondrial energy conversion and oxidative phosphorylation, Proc. Natl. Acad. Sci. U. S. A. 97 (2000) 12239–12243.
[69] S.A. Shoichet, A.T. Baumer, D. Stamenkovic, H. Sauer, A.F. Pfeiffer, C.R. Kahn, D. Muller-Wieland, C. Richter, M. Ristow, Frataxin promotes antioxidant defense in a thiol-dependent manner resulting in diminished malignant transformation in vitro, Hum. Mol. Genet. 11 (2002) 815–821.
[70] T.J. Schulz, R. Thierbach, A. Voigt, G. Drewes, B. Mietzner, P. Steinberg, A.F. Pfeiffer, M. Ristow, Induction of oxidative metabolism by mitochondrial frataxin inhibits cancer growth: Otto Warburg revisited, J. Biol. Chem. 281 (2006) 977–981.
[71] J.V. Llorens, J.A. Navarro, M.J. Martinez-Sebastian, M.K. Baylies, S. Schneuwly, J.A. Botella, M.D. Molto, Causative role of oxidative stress in a Drosophila model of Friedreich ataxia, FASEB J. 21 (2007) 333–344.
[72] M.A. Pook, S. Al-Mahdawi, C.J. Carroll, M. Cossee, H. Puccio, L. Lawrence, P. Clark, M. B. Lowrie, J.L. Bradley, J.M. Cooper, M. Koenig, S. Chamberlain, Rescue of the Friedreich's ataxia knockout mouse by human YAC transgenesis, Neurogenetics 3 (2001) 185–193.
[73] B. Schafer, Genetic conservation versus variability in mitochondria: the architecture of the mitochondrial genome in the petite-negative yeast Schizosaccharomyces pombe, Curr. Genet. 43 (2003) 311–326.
[74] W. Sun, Z. Wang, H. Jiang, J. Zhang, J. Bahler, D. Chen, A.I. Murchie, A novel function of the mitochondrial transcription factor Mtf1 in fission yeast; Mtf1 regulates the nuclear transcription of srk1, Nucleic Acids Res. 39 (2010) 2690–2700.
[75] P. Wu, R. Zhao, Y. Ye, J.Q. Wu, Roles of the DYRK kinase Pom2 in cytokinesis, mitochondrial morphology, and sporulation in fission yeast, PLoS One 6 (2011) e28000.
[76] H. Li, O. Gakh, D.Y.T. Smith, G. Isaya, Oligomeric yeast frataxin drives assembly of core machinery for mitochondrial iron–sulfur cluster synthesis, J. Biol. Chem. 284 (2009) 21971–21980.
[77] S.E. Faraj, L. Venturutti, E.A. Roman, C.B. Marino-Buslje, A. Mignone, S.C. Tosatto, J.M. Delfino, J. Santos, The role of the N-terminal tail for the oligomerization, folding and stability of human frataxin, FEBS Open Biol. 3 (2013) 310–320.
[78] K. Aloria, B. Schilke, A. Andrew, E.A. Craig, Iron-induced oligomerization of yeast frataxin homologue Yfh1 is dispensable in vivo, EMBO Rep. 5 (2004) 1096–1101.
[79] D.J. Wiley, P. Catanuto, F. Fontanesi, C. Rios, N. Sanchez, A. Barrientos, F. Verde, Bot1p is required for mitochondrial translation, respiratory function, and normal cell morphology in the fission yeast Schizosaccharomyces pombe, Eukaryot. Cell 7 (2008) 619–629.

[80] A.A. Starkov, The role of mitochondria in reactive oxygen species metabolism and signaling, Ann. N. Y. Acad. Sci. 1147 (2008) 37–52.
[81] N.D. Jhurry, M. Chakrabarti, S.P. McCormick, G.P. Holmes-Hampton, P.A. Lindahl, Biophysical investigation of the ironome of human jurkat cells and mitochondria, Biochemistry 51 (2012) 5276–5284.
[82] F. Auchere, R. Santos, S. Planamente, E. Lesuisse, J.M. Camadro, Glutathione-dependent redox status of frataxin-deficient cells in a yeast model of Friedreich's ataxia, Hum. Mol. Genet. 17 (2008) 2790–2802.
[83] M. Pandolfo, A. Pastore, The pathogenesis of Friedreich ataxia and the structure and function of frataxin, J. Neurol. 256 (Suppl. 1) (2009) 9–17.
[84] M.B. Delatycki, J. Camakaris, H. Brooks, T. Evans-Whipp, D.R. Thorburn, R. Williamson, S.M. Forrest, Direct evidence that mitochondrial iron accumulation occurs in Friedreich ataxia, Ann. Neurol. 45 (1999) 673–675.
[85] M. Whitnall, Y.S. Rahmanto, R. Sutak, X. Xu, E.M. Becker, M.R. Mikhael, P. Ponka, D.R. Richardson, The MCK mouse heart model of Friedreich's ataxia: alterations in iron-regulated proteins and cardiac hypertrophy are limited by iron chelation, Proc. Natl. Acad. Sci. U. S. A. 105 (2008) 9757–9762.
[86] G. Rustici, H. van Bakel, D.H. Lackner, F.C. Holstege, C. Wijmenga, J. Bahler, A. Brazma, Global transcriptional responses of fission and budding yeast to changes in copper and iron levels: a comparative study, Genome Biol. 8 (2007) R73.
[87] I. Fridovich, Superoxide radical and superoxide dismutases, Annu. Rev. Biochem. 64 (1995) 97–112.
[88] J. Park, S.P. McCormick, M. Chakrabarti, P.A. Lindahl, The lack of synchronization between iron uptake and cell growth leads to iron overload in Saccharomyces cerevisiae during post-exponential growth modes, Biochemistry 52 (2013) 9413–9425.